Title	Rapid detection of hypoxia-inducible factor-1-active tumours: pretargeted imaging with a protein degrading in a mechanism similar to hypoxia-inducible factor-1alpha
Author(s)	Ueda, Masashi; Kudo, Takashi; Kuge, Yuji; Mukai, Takahiro; Tanaka, Shotaro; Konishi, Hiroaki; Miyano, Azusa; Ono, Masahiro; Kizaka-Kondoh, Shinae; Hiraoka, Masahiro; Saji, Hideo
Citation	European journal of nuclear medicine and molecular imaging (2010), 37(8): 1566-1574
Issue Date	2010-08
URL	http://hdl.handle.net/2433/128622
Right	The original publication is available at www.springerlink.com
Type	Journal Article
Textversion	author

Title Page

Rapid detection of hypoxia-inducible factor-1-active tumors: Pretargeted imaging with a protein degrading in a mechanism similar to hypoxia-inducible factor-1α

Masashi Ueda[1,2], Takashi Kudo[2], Yuji Kuge[2,3], Takahiro Mukai[4], Shotaro Tanaka[5], Hiroaki Konishi[2], Azusa Miyano[2], Masahiro Ono[2], Shinae Kizaka-Kondoh[5], Masahiro Hiraoka[5], Hideo Saji[2]

[1]Radioisotopes Research Laboratory, Kyoto University Hospital, Faculty of Medicine, Kyoto University, 54 Shogoin Kawahara-cho, Kyoto 606-8507, Japan

[2]Department of Patho-Functional Bioanalysis, Kyoto University Graduate School of Pharmaceutical Sciences, 46-29 Yoshida-Shimo-Adachi-cho, Sakyo-ku, Kyoto 606-8501, Japan

[3]Central Institute of Isotope Science, Hokkaido University, Kita 15, Nishi 7, Kita-ku, Sapporo 060-0815, Japan

[4]Department of Biomolecular Recognition Chemistry, Graduate School of Pharmaceutical Sciences, Kyushu University, 3-1-1 Maidashi, Higashi-ku, Fukuoka 812-8582, Japan

[5]Department of Radiation Oncology and Image-applied Therapy, Kyoto University Graduate School of Medicine, 54 Kawahara-cho, Shogoin, Sakyo-ku, Kyoto 606-8507, Japan

Corresponding author;

Hideo Saji, PhD

Department of Patho-Functional Bioanalysis

Graduate School of Pharmaceutical Sciences

Kyoto University

46-29 Yoshida Shimoadachi-cho, Sakyo-ku, Kyoto 606-8501, Japan.

Phone: +81-75-753-4556, Fax: +81-75-753-4568

E-mail: hsaji@pharm.kyoto-u.ac.jp

Abstract

Purpose

Hypoxia-inducible factor-1 (HIF-1) plays an important role in malignant tumor progression. For the imaging of HIF-1-active tumors, we previously developed a protein—POS—which is effectively delivered to and selectively stabilized in HIF-1-active cells, and a radioiodinated biotin derivative—(3-^{123}I-iodobenzoyl)norbiotinamide (^{123}I-IBB)—which can bind to the streptavidin moiety of POS. In this study, we aimed to investigate the feasibility of the pretargeting method using POS and ^{123}I-IBB for early imaging of HIF-1-active tumors.

Methods

Tumor-implanted mice were pretargeted with POS. After 24 h, ^{125}I-IBB was administered and subsequently, the biodistribution of radioactivity was investigated at several time points. *In vivo* planar imaging, comparison between ^{125}I-IBB accumulation and HIF-1 transcriptional activity, and autoradiography were performed at 6 h after the administration of ^{125}I-IBB, which was administered 24 h after the administration of POS. The same sections that were used in autoradiographic analysis were subjected to HIF-1α immunohistochemistry.

Results

^{125}I-IBB accumulation was observed in tumors of mice pretargeted with POS (1.6% injected dose/g (%ID/g) at 6 h). This result is comparable to the data derived from ^{125}I-IBB-conjugated POS-treated mice (1.4%ID/g at 24 h). *In vivo* planar imaging provided clear tumor images. The tumoral accumulation of

^{125}I-IBB significantly correlated with HIF-1-dependent luciferase bioluminescence (R = 0.84, P < 0.01). The intratumoral distribution of ^{125}I-IBB was heterogenous and significantly correlated with HIF-1α-positive regions (R = 0.58, P < 0.0001).

Conclusion

POS pretargeting with ^{123}I-IBB is a useful technique in the rapid imaging and detection of HIF-1-active regions in tumors.

Key Words;

Tumor hypoxia, Hypoxia-inducible Factor-1 (HIF-1), Oxygen-dependent degradation (ODD), Molecular imaging, Pretargeting

Introduction

Insufficient blood supply to a rapidly growing tumor leads to the presence of an oxygen tension below physiological levels, hypoxia in solid tumors [1]. Tumor hypoxia is critically important in tumor physiology and cancer treatment, and it appears to be strongly associated with malignant progression and therapy resistance. The transcription factor, hypoxia-inducible factor-1 (HIF-1) is induced in a hypoxic region; it is a master regulator of the genes that encode for angiogenic and metastatic factors, and plays an important role in tumor progression [2-4]. Thus, noninvasive imaging of HIF-1-active regions in tumors will be useful for characterizing tumors and determining a course of therapy.

HIF-1 is a heterodimer that consists of an oxygen-sensitive alpha subunit (HIF-1α) and a constitutively expressed beta subunit. In normoxia, two proline residues in the oxygen-dependent degradation domain (ODD) of HIF-1α are hydroxylated, leading to a proteasomal degradation of HIF-1α. Under hypoxic conditions, oxygen is the rate-limiting factor for proryl hydroxylation, resulting in a decreased degradation of HIF-1α [5, 6]. That is to say, the ODD of HIF-1α is responsible for the regulation of HIF-1 activity. Thus, it is likely that a probe containing ODD and degrading in a manner similar to HIF-1α does can be used to evaluate HIF-1 activity *in vivo*.

We have recently developed proteins in which the protein transduction domain (PTD) is fused to the ODD and demonstrated the specificity of these proteins to HIF-1-active cells [7-11]. In a previous study, we have also fused the PTD-ODD with a monomeric streptavidin (SAV), to produce a chimeric protein, PTD-ODD-SAV (POS); we also synthesized a radiolabeled biotin derivative,

(3-$^{123/125}$I-iodobenzoyl)norbiotinamide ($^{123/125}$I-IBB). For nuclear medical imaging, the two were conjugated ($^{123/125}$I-IPOS); the characterization thereof has been presented previously [9]. In brief, POS was degraded in an oxygen-dependent manner and a clear tumor image was obtained 24 h post-injection of ^{123}I-IPOS; additionally, the tumoral accumulation correlated with HIF-1 activity and the intratumoral distribution of ^{125}I-IPOS was heterogeneous and corresponded to hypoxic areas. These findings suggested that ^{123}I-IPOS is a potential probe for the imaging of HIF-1-active tumors. However, due to its large molecular size, ^{123}I-IPOS cleared from the blood slowly; thus, we could not obtain a high tumor-to-normal tissue ratio within a short time after probe injection.

To overcome this problem, we propose a pretargeting method based on the high-affinity interaction between streptavidin and biotin [12]. This method uses a combination of tumor-seeking molecules and the prompt clearance of low-molecular-weight radiolabeled compounds (effector molecules) that are cleared within minutes from the blood. One of the advantages of the pretargeting method is that this method provides a high tumour-to-normal tissue ratio within a short time after injection. In addition, because the effector molecules used in this method are rapidly cleared from the body, the radiation exposure reduces. Moreover, some recent studies have shown that the tumor uptake of the effector molecules used in the pretargeting method was achieved identical to or even higher than that of directly radiolabeled antibody. The images and therapeutic effects reported by these studies were significantly improved [13-15]. In the present study, we aimed to reveal the effectiveness of the pretargeting method using POS and ^{123}I-IBB, in the rapid imaging of HIF-1-active tumor hypoxia.

Materials and Methods

Cell and cell culture

FM3A mouse mammary tumor cells were purchased from Health Science Research Resources Bank (Osaka, Japan) and were cultured in 10% fetal bovine serum (FBS)-RPMI 1640 medium (Nissui Pharmaceutical, Tokyo, Japan). Suit2 human pancreatic tumor cells that express luciferase in response to HIF-1 activity (Suit2/Luc cells) were established by Prof. Kizaka-Kondoh [16]. These cells were authenticated by multi plex PCR method using short tandem repeat and were maintained in 10% FBS-Dulbecco's modified Eagle's medium (Nissui Pharmaceutical). The culture media were supplemented with penicillin (100 units/mL) and streptomycin (100 μg/mL). Cells were incubated at 37°C in a well-humidified incubator with 5% CO_2 and 95% air.

Preparation of fusion protein

POS was overexpressed in *Escherichia coli* and purified as described in a previous report [9]. Purified POS was then dissolved in Tris-HCl buffer (pH 8.0).

Synthesis

Ammonium ^{123}I-iodide was kindly provided by Nihon Medi-Physics (Hyogo, Japan). Sodium

^{125}I-iodide was purchased from PerkinElmer Life and Analytical Sciences (Boston, MA). All other chemicals used in this study were of reagent grade and are commercially available. $^{123/125}$I-IBB and non-radioactive IBB were synthesized as described in a previous report [9, 17]. ^{123}I-IPOS was obtained by incubating ^{123}I-IBB and POS for 1 h, followed by purification with Sephadex G50 columns (GE Healthcare Bioscience, Uppsala, Sweden).

Animal model

Animal studies were conducted in accordance with our institutional guidelines, and the experimental procedures were approved by the Kyoto University Animal Care Committee. Five-week-old female C3H/He mice and BALB/c *nu/nu* mice were purchased from Japan SLC, Inc. (Hamamatsu, Japan). FM3A and Suit2/Luc tumor models were prepared as described in a previous report [9]. The cells were subcutaneously implanted in the right thighs, except in the case of the mice that were used for the bioluminescence imaging wherein the cells were subcutaneously implanted in both the thighs. After tumor implantation, mice were fed an AIN76-A-based, biotin-free diet (Oriental Yeast Co. Ltd., Tokyo, Japan) in order to prevent dietary biotin from inhibiting the binding of ^{125}I-IBB to POS. The mice were subjected to a tracer study two weeks after implantation. The average diameter and average volume of the tumors were 8 mm and 350 mm^3, respectively.

Biodistribution

^{125}I-IBB (37 kBq) was injected intravenously into FM3A-implanted mice (n = 3–5); at 1, 3, 6, and 24 h post-injection, the mice were sacrificed. For the pretargeting study, the mice (n = 5) were injected with 30 μg of POS and 24 h later, ^{125}I-IBB was injected intravenously. The mice were sacrificed at the same time points as described above. Whole organ specimens were immediately removed and weighed, and their radioactivity was measured with an auto well gamma counter (ARC2000; Aloka, Co., Ltd., Tokyo, Japan). The results are expressed in terms of the percent injected dose per gram of tissue (%ID/g).

In vivo blocking study

FM3A-implanted mice (n = 5) were pretargeted with POS (30 μg); 24 h later, ^{125}I-IBB (37 kBq) was injected intravenously, with or without D-biotin (1 nmol) or with unlabeled IBB (500 pmol). Six hours after ^{125}I-IBB administration, the mice were sacrificed. Whole organ specimens were immediately removed and weighed, and their radioactivity was measured with the gamma counter (ARC2000). The results are expressed as %ID/g.

Size-exclusion analysis of radioactive compounds in tumors

FM3A-implanted mice (n = 5) were pretargeted with POS (30 μg); 24 h later, ^{125}I-IBB (8.0 MBq) was injected intravenously. The mice were sacrificed 6 h after the injection of ^{125}I-IBB, and the tumors were then removed. Extracts were prepared according to a previously reported method [18], with a slight modification. In brief, the tumors were homogenized in ice-cold 0.1 M Tris-HCl buffer containing 0.15 M

NaC1 (pH 6.5), using a Polytron homogenizer (PT10-35, Kinematica AG, Switzerland); the preparations were then centrifuged at 4°C and 5,000 × *g* for 30 min (Micro Cooling Centrifuge 5922; Kubota, Osaka, Japan). The supernatants were filtered through a 0.46-μm filter (Nacalai Tesque, Kyoto, Japan) and analyzed by size-exclusion chromatography using a PD-10 column (GE Healthcare Bioscience).

In vivo imaging

SPECT-2000H scanner (Hitachi Medical Co., Tokyo, Japan) employing a low-energy, high-resolution, parallel-hole collimator [19, 20] was used. For direct targeting (*n* = 4), ^{123}I-IPOS (30 μg, 4.9–7.4 MBq) was injected intravenously into each FM3A-implanted mouse. For the pretargeting method (*n* = 5), ^{123}I-IBB (3.1–16 MBq) was injected into a tail vein 24 h after pretargeting with POS (30 μg). Under 2.5% of halothane anesthesia, the mice were placed on a scanner bed in the prone position. Planar images were obtained at 24 h after the injection of ^{123}I-IPOS in mice belonging to the direct-targeted group or at 6 h after the injection of ^{123}I-IBB in mice belonging to the pretargeted group. The image-acquisition time was 10 min for both the groups. Regions of interest (ROI) were set on the tumor in the right thigh and the corresponding area in the left thigh.

Comparison between ^{125}I-IBB accumulationin and HIF-1 transcriptional activity within identical tumors in mice pretargeted with POS

The Suit2/Luc-implanted mice (*n* = 5) were pretargeted with POS (30 μg) and 24 h later, ^{125}I-IBB

(37 kBq) was injected intravenously. After 5.5 h, 200 μL of D-luciferin solution (10 mg/mL in PBS; VivoGlo Luciferin, Promega, Wisconsin) was injected intraperitoneally. After 20 min, the mice were anesthetized with 2.5% isoflurane and imaged according to a previously described method [9]. After bioluminescence imaging, the mice were sacrificed and the radioactivity in each tumor was measured.

Autoradiography

Autoradiographic studies were performed in Suit2/Luc-implanted mice (n = 6). The mice were pretargeted with POS (30 μg) and 24 h later, ^{125}I-IBB (4.1 MBq) was injected intravenously. After another 4 h, pimonidazole (PIMO, 60 mg/kg) was injected intraperitoneally and the mice were sacrificed 2 h later. Autoradiograms were then obtained and analyzed, according to a previously described method [19-21]. The adjacent section on each autoradiogram was stained with hematoxylin–eosin to identify regions of necrosis.

Immunohistochemistry

The slides used in the autoradiographic study were subjected to dual fluorescent immunostaining for HIF-1α and PIMO. The sections were fixed in 2% paraformaldehyde and ice-cold methanol, blocked with Protein Block Serum Free (Dako, Glostrup, Denmark), and treated with anti-human/mouse HIF-1α polyclonal antibody (R&D Systems, Minneapolis, MN) as a primary antibody; the specific signals were detected using an Alexa Fluor 568-conjugated F(ab′)$_2$ fragment of goat anti-rabbit antibody (Invitrogen,

San Diego, CA). Thereafter, after washing with PBS, FITC-conjugated mouse IgG_1 monoclonal antibody (Chemicon, Temecula, CA) was treated according to the manufacturer's protocol for PIMO staining. The sections were then dried and coverslipped using an antifade reagent (ProLong Gold; Invitrogen). To evaluate the specificity of the HIF-1α signal, negative control rabbit immunoglobulin (Dako) was incubated with the adjacent sections, instead of the primary antibody. To evaluate the specificity of the PIMO signal, tumor sections derived from PIMO-untreated mice were stained by following the same protocol. Fluorescent microscopic images were obtained by BIOREVO BZ-9000 (Keyence Corp., Osaka, Japan).

Image analysis

The autoradiograms were quantified using MultiGauge software (ver. 3.0, Fuji Photo Film Co., Ltd., Tokyo, Japan) and the immunohistochemical images were analyzed using BZ analyzer software (Keyence Corp.). ROIs were set on identical positions in both images on the basis of the x- and y-position of each ROI displayed in the both softwares. The necrotic regions were excluded from the analysis. We set 10–14 ROIs (area, 1-mm^2) on the autoradiogram of each tumor and then transferred them to the corresponding immunohistochemical image. The radioactivity in each ROI was expressed in terms of %ID. The expression densities of HIF-1α and PIMO were determined in terms of the percentage of the positively stained region.

Statistical analyses

Comparisons between the two groups were made using the Mann-Whitney *U* test, and correlation coefficients were assessed using the Spearman rank analysis. A Chi-square test was used to compare the correlation coefficients between ^{125}I-IBB accumulation and HIF-1α expression or PIMO adduct-formation. $P < 0.05$ was considered statistically significant.

Results

Radiosynthesis of $^{123/125}$I-IBB and ^{123}I-IPOS

^{123}I-IBB and ^{125}I-IBB were obtained in the absence of a carrier and with radiochemical yields of 29% and 65% and radiochemical purities of greater than 95% and greater than 94%, respectively. ^{123}I-IPOS was obtained with a radiochemical yield of 90% and a radiochemical purity of greater than 99%.

Biodistribution

An examination of the biodistribution of ^{125}I-IBB alone revealed that the tumor-to-blood ratio was less than 1 at all time points. This indicated that ^{125}I-IBB did not accumulate in the tumors. The radioactivity in the stomach was low; this indicates the resistance of ^{125}I-IBB to deiodination *in vivo* (Table 1). In contrast, in the pretargeted group, the tumor-to-blood ratio was greater than 1 as early as 1 h after the injection of ^{125}I-IBB and the tumor-to-blood ratio had increased in a time-dependent manner (Table 2). The

blood clearance in both groups was comparable. In the pretargeted group, tumor accumulation of ^{125}I-IBB at 6 h post-injection was 1.58 ± 0.42%ID/g, which was more than 30-fold higher than the case of ^{125}I-IBB alone (0.05 ± 0.01%ID/g). The radioactivity in the normal tissues decreased more rapidly than that in the tumor. The radioactivity in the tumor at 24 h after injection was the second highest among organs examined and both the tumor-to-blood and tumor-to-muscle ratios further increased (Table 2).

The tumoral uptake of ^{125}I-IBB was significantly reduced to 46%, through the treatment with non-radioactive IBB (Table 3). A concomitant treatment with D-biotin also resulted in a 37% decrease in the tumoral uptake of ^{125}I-IBB (Data not shown). The ^{125}I-IBB accumulation in other tissues, except in blood, decreased on the treatment with non-radioactive IBB.

Size-exclusion analysis of radioactive compounds in tumors

The recovery of radioactivity from tumor homogenates was 95.7 ± 7.2%, and that from the PD-10 columns was 85.5 ± 6.9%. A major proportion of the radioactivity was eluted in a macromolecular fraction (78.7 ± 6.7%).

In vivo imaging

Fig. 1A illustrates the accumulation of ^{123}I-IBB in the POS-pretargeted tumor. The tumor was clearly visualized 6 h after ^{123}I-IBB injection, and the calculated tumor-to-muscle ratio was 4.6 ± 1.4. The image was comparable to that obtained 24 h after ^{123}I-IPOS injection, using the direct-targeting method

(Fig. 1B; tumor-to-muscle ratio, 6.9 ± 1.6). Compared to the direct targeting method, with the pretargeting method, radioactivity in the liver decreased, but increased in the intestine. These findings were consistent with the biodistribution study data.

^{125}I-IBB accumulation vs. HIF-1 transcriptional activity in tumors in mice pretargeted with POS

Figure 2 shows a positive correlation between HIF-1-induced luciferase bioluminescence and ^{125}I-IBB accumulation at 6 h post-injection in tumors in mice pretargeted with POS ($R = 0.84$, $P < 0.01$).

Regional distribution of ^{125}I-IBB in the POS-pretargeted tumor

Dual fluorescent immunohistochemistry revealed the presence of HIF-1α- and PIMO-positive hypoxic areas in the tumor (Fig. 3A, B). The sections derived from PIMO-untreated mice were not stained with anti-PIMO antibody, and the HIF-1α signal was not detected in the negative control antibody-treated sections (data not shown). The autoradiogram showed that the distribution of ^{125}I-IBB in the tumor was heterogeneous (Fig. 3C) and, for the most part, corresponded to the HIF-1α- or PIMO-positive hypoxic areas. However, there were also a few regions where the signal of HIF-1α or PIMO was positive, but where ^{125}I-IBB had not accumulated (Fig. 3D, E). High-magnification merged imaging of HIF-1α and PIMO immunostaining revealed that HIF-1α-positive regions and PIMO-positive regions were not always identical; some regions were positive for both, while other regions did not match (Fig. 3F). Therefore, we compared correlations between ^{125}I-IBB accumulation and expressions of HIF-1α or PIMO. As shown in

Fig. 4, significantly positive correlations were found between the regional accumulation of ^{125}I-IBB in POS-pretargeted tumor sections and the expression of both hypoxic markers (HIF-1α: $R = 0.58$, $P < 0.0001$; PIMO: $R = 0.34$, $P < 0.005$). The correlation coefficient between ^{125}I-IBB and HIF-1α was greater than that with PIMO, though the difference was not statistically significant ($\chi^2 = 3.13$, $P = 0.077$).

Discussion

Here we show early-phase tumor imaging afforded by pretargeting using POS and $^{123/125}$I-IBB. Using the pretargeting method, the tumoral accumulation (1.6%ID/g) and the tumor-to-blood ratio (4.2) at 6 h post-injection were found to be comparable to the data obtained 24 h after ^{125}I-IPOS injection (1.4%ID/g, 5.1) [9]. The scintigraphic images of mice targeted with ^{123}I-IPOS were very similar to those of prior studies, in which high signal levels were detected in the tumor—although the highest activity accumulated in the liver, even 24 h post-injection [9]. In contrast, the images of the pretargeted mice clearly demonstrate that ^{123}I-IBB accumulated in the tumor more rapidly and cleared much more promptly from the body—with the exception of the intestine—than did the ^{123}I-IPOS. These results indicate that the pretargeting method allows a shortening of the waiting time to one-fourth that required by direct targeting, in obtaining an adequate image. Clinical application of the pretargeting method in the future will contribute to reduction in radiation exposure of a patient.

Recently, it has been suggested that HIF-1 activates a number of genes—such as VEGF,

erythropoietin, matrix metalloproteinase, and glucose transporter—and that the expression level of HIF-1 correlates with poor prognosis in many tumors [22-26]. Furthermore, the activation of such genes has an important role with respect to aggressive cancer phenotypes. Therefore, visualization and tumor therapy targeting for HIF-1 activation may be an important supplement to imaging of hypoxia per se, when characterizing tumors. Thus far, some hypoxia imaging probes—such as ^{18}F-fluoromisonidazole (^{18}F-FMISO), 1-α-D-(5-deoxy-5-^{18}F-fluoroarabinofuranosyl)-2-nitroimidazole (^{18}F-FAZA), and ^{64}Cu-diacetyl-bis(*N*^{4}-methylthiosemicarbazone) (^{64}Cu-ATSM)—have been developed [27]. They detect physically low oxygen pressure (<10 mmHg) and are useful in predicting efficacy of radiotherapy [28]. However, the mechanisms underlying hypoxic accumulation of such probes are not dependent on HIF-1 expression [29]. Previously reported HIF-1-activity imaging systems required exogenous reporter gene transcription, which presents difficulties in practice [30, 31]. In contrast, our approach could assess HIF-1-activity directly, via a two-step targeting of the probes.

A recent immunohistochemical study has demonstrated the lack of complete colocalization between HIF-1α and PIMO. Sobhanifar *et al.* report that HIF-1 expressed at higher levels of oxygen than those that allow PIMO metabolism and binding [32]. Thus, we compared the correlation between ^{125}I-IBB accumulation and HIF-1α- or PIMO-positive regions. As shown in Fig. 4, the correlation coefficient between ^{125}I-IBB and HIF-1α was greater than was the case with PIMO, although the difference between the 2 correlation coefficients was not statistically significant. Therefore, the ^{125}I-IBB-accumulated regions potentially corresponded to the HIF-1α-positive regions but to a lesser degree with the PIMO-positive

regions. However, in the present study, the HIF-1α-positive region was mainly detected both in the PIMO-positive regions and in the regions surrounding them (Fig. 3F). The result is consistent with that of a previous study, which reports that carbonic anhydrase 9, a HIF-1-regulated protein, generally colocated with PIMO though displaying greater extension in the direction of perfused areas [33]. Due to the overlap, the ^{125}I-IBB-accumulated region also showed a weak positive correlation with the PIMO-positive regions. On the other hand, there were a few HIF-1α-negative regions in which ^{125}I-IBB accumulated (Fig. 3D). This discrepancy could be explained by the delivery of POS and/or ^{125}I-IBB. Since both probes were delivered by blood flow, they potentially tend to accumulate in blood-vessel-rich regions, i.e., HIF-1α-negative regions. Because the degradation rate of POS was relatively slow [9], an excess amount of POS delivered to HIF-1α-negative regions could not be degraded, resulting in ^{125}I-IBB accumulation in those regions. POS contains not only the essential domain related to the oxygen-dependent degradation of HIF-1α, but also PTD and SAV. These modifications may lower the rate of degradation, and this is a drawback of POS. However, it should be noted that by using the pretargeting method with POS and ^{123}I-IBB, the radioactivity accumulation significantly correlated with the HIF-1α-positive region (Fig. 4A). Furthermoer, the accumulation of ^{123}I-IBB correlated with HIF-1 transcriptional activity in the tumors in mice pretargeted with POS (Fig. 2). Thus, our approach would detect not only hypoxic regions, but also HIF-1-active regions; thus, this approach could prove important to the qualitative diagnosis of and effective therapy against cancer.

In the pretargeting study, ^{125}I-IBB accumulated in the tumors of POS-pretargeted mice. The

accumulation was inhibited by non-radioactive IBB or D-biotin. Moreover, most of the radioactivity in the tumor existed as macromolecules. Taken together, the radioactivity in the tumor is caused by the binding of ^{125}I-IBB to the SAV moiety of POS. Thus, ^{125}I-IBB has the ability to bind to streptavidin, not only *in vitro* but also *in vivo*. It was reported that the expression of HIF-1 is not ubiquitous, but heterogeneous, and is small in tumors [34]. The probe accumulation in the tumors harboring HIF-1-dependent reporter genes was approximately 1%ID/g in previous studies [34-36], which is comparable to the results of the present study.

In the biodistribution study of ^{125}I-IBB alone, the accumulation of radioactivity was highest in the intestine. This tissue distribution pattern reflects the behavior of radioiodinated biotin itself, since ^{125}I-IBB is not subjected to cleavage by serum biotinidase [17]. The high accumulation of ^{125}I-IBB in the intestine resulted in high background activity in the abdominal region; therefore, the imaging of abdominal HIF-1-active tumors would be difficult. In this case, biotin derivatives those show faster clearance from the abdominal region than ^{125}I-IBB is required. However, the background radioactivity in the thoracic region and cervicofacial region was considerably low. The expression of HIF-1 has been reported to be associated with a poor prognosis in breast and lung cancers and in head and neck squamous cell carcinomas [26, 37, 38]; therefore, our imaging approach would be particularly useful for detecting HIF-1 activity in those tumors.

Recent studies have revealed that HIF-1 level is controlled not only at the post-transcriptional level—that is, the oxygen-dependent regulation of the HIF-1α—but also at the transcriptional and translational levels [39, 40]. In a region where the transcription and translation of HIF-1α increased, an

excess amount of HIF-1α was likely to saturate the ubiquitin-proteasome degradation system and result in the upregulation of HIF-1, even in mild hypoxic conditions. This may be one reason why the threshold of oxygen pressure for HIF-1 stabilization is ambiguous and depends upon the character of the organs or tumors. In such regions, the POS degradation rate would also decrease, because it contains the ODD and degrades in the same manner as HIF-1α. Thus, in imaging with POS-pretargeting and ^{123}I-IBB, it is possible to depict HIF-1-active regions that result from either hypoxic stabilization or the upregulation of transcription and translation.

Conclusion

Using the pretargeting method, clear tumor images were obtained in a shorter period of time than was possible with the direct-labeling method. Intratumoral accumulations of ^{125}I-IBB in the POS-pretargeted tumors significantly correlated with HIF-1α-positive regions. These findings demonstrate that the pretargeting method with POS and ^{123}I-IBB is effective for the rapid imaging of HIF-1-active tumor hypoxia.

Acknowledgement

The authors would like to thank Nihon Medi-Physics for providing ammonium ^{123}I-iodide. This work was supported in part by “R&D of Molecular Imaging Equipment for Malignant Tumor Therapy Support” by New Energy and Industrial Technology Development Organization (NEDO), Japan; Health Labour Sciences Research Grant for Research on Advanced Medical Technology from the Ministry of Health, Labour and Welfare of Japan; and a Grant-in-Aid for Exploratory Research (17659010) and a Grant-in-Aid for Young Scientists (B) (21791187) from the Ministry of Education, Culture, Sports, Science and Technology of Japan.

Conflict of interest

The authors have no conflict of interest.

References

1. Vaupel P, Kallinowski F, Okunieff P. Blood flow, oxygen and nutrient supply, and metabolic microenvironment of human tumors: a review. Cancer Res. 1989;49:6449-65.

2. Semenza GL. Expression of hypoxia-inducible factor 1: mechanisms and consequences. Biochem Pharmacol. 2000;59:47-53.

3. Wenger RH. Cellular adaptation to hypoxia: O_2-sensing protein hydroxylases, hypoxia-inducible transcription factors, and O_2-regulated gene expression. Faseb J. 2002;16:1151-62.

4. Ballinger JR. Imaging hypoxia in tumors. Semin Nucl Med. 2001;31:321-9.

5. Kizaka-Kondoh S, Inoue M, Harada H, Hiraoka M. Tumor hypoxia: a target for selective cancer therapy. Cancer Sci. 2003;94:1021-8.

6. Jiang BH, Semenza GL, Bauer C, Marti HH. Hypoxia-inducible factor 1 levels vary exponentially over a physiologically relevant range of O_2 tension. Am J Physiol. 1996;271:C1172-80.

7. Harada H, Kizaka-Kondoh S, Li G, Itasaka S, Shibuya K, Inoue M, et al. Significance of HIF-1-active cells in angiogenesis and radioresistance. Oncogene. 2007;26:7508-16.

8. Harada H, Kizaka-Kondoh S, Hiraoka M. Optical imaging of tumor hypoxia and evaluation of efficacy of a hypoxia-targeting drug in living animals. Mol Imaging. 2005;4:182-93.

9. Kudo T, Ueda M, Kuge Y, Mukai T, Tanaka S, Masutani M, et al. Imaging of HIF-1-active tumor hypoxia using a protein effectively delivered to and specifically stabilized in HIF-1-active tumor

cells. J Nucl Med. 2009;50:942-9.

10. Kizaka-Kondoh S, Konse-Nagasawa H. Significance of nitroimidazole compounds and hypoxia-inducible factor-1 for imaging tumor hypoxia. Cancer Sci. 2009;100:1366-73.

11. Kizaka-Kondoh S, Tanaka S, Harada H, Hiraoka M. The HIF-1-active microenvironment: an environmental target for cancer therapy. Adv Drug Deliv Rev. 2009;61:623-32.

12. Green NM. Avidin. 3. the Nature of the Biotin-Binding Site. Biochem J. 1963;89:599-609.

13. Goldenberg DM, Rossi EA, Sharkey RM, McBride WJ, Chang CH. Multifunctional antibodies by the Dock-and-Lock method for improved cancer imaging and therapy by pretargeting. J Nucl Med. 2008;49:158-63.

14. Sharkey RM, Cardillo TM, Rossi EA, Chang CH, Karacay H, McBride WJ, et al. Signal amplification in molecular imaging by pretargeting a multivalent, bispecific antibody. Nat Med. 2005;11:1250-5.

15. Sharkey RM, Karacay H, Litwin S, Rossi EA, McBride WJ, Chang CH, et al. Improved therapeutic results by pretargeted radioimmunotherapy of non-Hodgkin's lymphoma with a new recombinant, trivalent, anti-CD20, bispecific antibody. Cancer Res. 2008;68:5282-90.

16. Kizaka-Kondoh S, Itasaka S, Zeng L, Tanaka S, Zhao T, Takahashi Y, et al. Selective killing of hypoxia-inducible factor-1-active cells improves survival in a mouse model of invasive and metastatic pancreatic cancer. Clin Cancer Res. 2009;15:3433-41.

17. Foulon CF, Alston KL, Zalutsky MR. Synthesis and preliminary biological evaluation of

(3-iodobenzoyl)norbiotinamide and ((5-iodo-3-pyridinyl)carbonyl)norbiotinamide: two radioiodinated biotin conjugates with improved stability. Bioconjug Chem. 1997;8:179-86.

18. Motta-Hennessy C, Sharkey RM, Goldenberg DM. Metabolism of indium-111-labeled murine monoclonal antibody in tumor and normal tissue of the athymic mouse. J Nucl Med. 1990;31:1510-9.

19. Ishino S, Kuge Y, Takai N, Tamaki N, Strauss HW, Blankenberg FG, et al. ^{99m}Tc-Annexin A5 for noninvasive characterization of atherosclerotic lesions: imaging and histological studies in myocardial infarction-prone Watanabe heritable hyperlipidemic rabbits. Eur J Nucl Med Mol Imaging. 2007;34:889-99.

20. Ishino S, Mukai T, Kuge Y, Kume N, Ogawa M, Takai N, et al. Targeting of lectinlike oxidized low-density lipoprotein receptor 1 (LOX-1) with ^{99m}Tc-labeled anti-LOX-1 antibody: potential agent for imaging of vulnerable plaque. J Nucl Med. 2008;49:1677-85.

21. Ueda M, Iida Y, Tominaga A, Yoneyama T, Ogawa M, Magata Y, et al. Nicotinic acetylcholine receptors expressed in the ventral posterolateral thalamic nucleus play an important role in antiallodynic effects. Br J Pharmacol. 2010; doi:10.1111/j.1476-5381.2009.00613.x.

22. Harada H, Xie X, Itasaka S, Zeng L, Zhu Y, Morinibu A, et al. Diameter of tumor blood vessels is a good parameter to estimate HIF-1-active regions in solid tumors. Biochem Biophys Res Commun. 2008;373:533-8.

23. Marignol L, Coffey M, Lawler M, Hollywood D. Hypoxia in prostate cancer: a powerful shield

against tumour destruction? Cancer Treat Rev. 2008;34:313-27.

24. Ke HL, Wei YC, Yang SF, Li CC, Wu DC, Huang CH, et al. Overexpression of hypoxia-inducible factor-1alpha predicts an unfavorable outcome in urothelial carcinoma of the upper urinary tract. Int J Urol. 2008;15:200-5.

25. Miyake K, Yoshizumi T, Imura S, Sugimoto K, Batmunkh E, Kanemura H, et al. Expression of hypoxia-inducible factor-1alpha, histone deacetylase 1, and metastasis-associated protein 1 in pancreatic carcinoma: correlation with poor prognosis with possible regulation. Pancreas. 2008;36:e1-9.

26. Trastour C, Benizri E, Ettore F, Ramaioli A, Chamorey E, Pouyssegur J, et al. HIF-1alpha and CA IX staining in invasive breast carcinomas: prognosis and treatment outcome. Int J Cancer. 2007;120:1451-8.

27. Mees G, Dierckx R, Vangestel C, Van de Wiele C. Molecular imaging of hypoxia with radiolabelled agents. Eur J Nucl Med Mol Imaging. 2009;36:1674-86.

28. Dunphy MP, Lewis JS. Radiopharmaceuticals in preclinical and clinical development for monitoring of therapy with PET. J Nucl Med. 2009;50 Suppl 1:106S-21S.

29. Krohn KA, Link JM, Mason RP. Molecular imaging of hypoxia. J Nucl Med. 2008;49 Suppl 2:129S-48S.

30. He F, Deng X, Wen B, Liu Y, Sun X, Xing L, et al. Noninvasive molecular imaging of hypoxia in human xenografts: comparing hypoxia-induced gene expression with endogenous and exogenous

hypoxia markers. Cancer Res. 2008;68:8597-606.

31. Yeom CJ, Chung JK, Kang JH, Jeon YH, Kim KI, Jin YN, et al. Visualization of hypoxia-inducible factor-1 transcriptional activation in C6 glioma using luciferase and sodium iodide symporter genes. J Nucl Med. 2008;49:1489-97.

32. Sobhanifar S, Aquino-Parsons C, Stanbridge EJ, Olive P. Reduced expression of hypoxia-inducible factor-1alpha in perinecrotic regions of solid tumors. Cancer Res. 2005;65:7259-66.

33. Li XF, Carlin S, Urano M, Russell J, Ling CC, O'Donoghue JA. Visualization of hypoxia in microscopic tumors by immunofluorescent microscopy. Cancer Res. 2007;67:7646-53.

34. Serganova I, Doubrovin M, Vider J, Ponomarev V, Soghomonyan S, Beresten T, et al. Molecular imaging of temporal dynamics and spatial heterogeneity of hypoxia-inducible factor-1 signal transduction activity in tumors in living mice. Cancer Res. 2004;64:6101-8.

35. Hsieh CH, Kuo JW, Lee YJ, Chang CW, Gelovani JG, Liu RS. Construction of mutant TKGFP for real-time imaging of temporal dynamics of HIF-1 signal transduction activity mediated by hypoxia and reoxygenation in tumors in living mice. J Nucl Med. 2009;50:2049-57.

36. Wen B, Burgman P, Zanzonico P, O'Donoghue J, Cai S, Finn R, et al. A preclinical model for noninvasive imaging of hypoxia-induced gene expression; comparison with an exogenous marker of tumor hypoxia. Eur J Nucl Med Mol Imaging. 2004;31:1530-8.

37. Ioannou M, Papamichali R, Kouvaras E, Mylonis I, Vageli D, Kerenidou T, et al. Hypoxia

inducible factor-1 alpha and vascular endothelial growth factor in biopsies of small cell lung carcinoma. Lung. 2009;187:321-9.

38. van den Broek GB, Wildeman M, Rasch CR, Armstrong N, Schuuring E, Begg AC, et al. Molecular markers predict outcome in squamous cell carcinoma of the head and neck after concomitant cisplatin-based chemoradiation. Int J Cancer. 2009;124:2643-50.

39. North S, Moenner M, Bikfalvi A. Recent developments in the regulation of the angiogenic switch by cellular stress factors in tumors. Cancer Lett. 2005;218:1-14.

40. Skinner HD, Zheng JZ, Fang J, Agani F, Jiang BH. Vascular endothelial growth factor transcriptional activation is mediated by hypoxia-inducible factor 1alpha, HDM2, and p70S6K1 in response to phosphatidylinositol 3-kinase/AKT signaling. J Biol Chem. 2004;279:45643-51.

Tables

Table 1. Biodistribution of ^{125}I-IBB in FM3A-implanted mice

	Time after injection (h)			
Organ	1	3	6	24
Blood	1.12 ± 0.43	0.33 ± 0.01	0.15 ± 0.00	0.03 ± 0.01
Liver	6.36 ± 1.70	1.21 ± 0.04	0.20 ± 0.04	0.02 ± 0.01
Heart	1.27 ± 0.31	0.26 ± 0.01	0.07 ± 0.04	0.02 ± 0.02
Lung	1.14 ± 0.22	0.30 ± 0.04	0.10 ± 0.03	0.02 ± 0.01
Kidney	5.54 ± 0.74	1.06 ± 0.23	0.35 ± 0.18	0.07 ± 0.02
Stomach	0.62 ± 0.13	0.35 ± 0.23	0.33 ± 0.24	0.12 ± 0.10
Intestine	32.61 ± 8.24	24.73 ± 12.12	10.69 ± 4.93	0.95 ± 0.64
Tumor	0.53 ± 0.14	0.13 ± 0.04	0.05 ± 0.01	0.01 ± 0.01
Muscle	0.84 ± 0.18	0.15 ± 0.05	0.03 ± 0.02	0.01 ± 0.01
Tumor/Blood	0.49 ± 0.14	0.39 ± 0.09	0.36 ± 0.09	0.57 ± 0.57

Organ uptake values are expressed as the percent injected dose per gram of tissue, except in the case of the stomach (the percent injected dose) and tumor/blood ratio. Values are represented as the mean ± S.D., n = 3–5.

Table 2. Biodistribution of ^{125}I-IBB in FM3A-implanted mice pretargeted with POS

	Time after injection (h)			
Organ	1	3	6	24
Blood	1.28 ± 0.22	0.58 ± 0.05	0.37 ± 0.05	0.05 ± 0.01
Liver	10.16 ± 0.98	5.56 ± 0.74	4.07 ± 0.38	0.57 ± 0.15
Heart	1.77 ± 0.11	0.90 ± 0.12	0.59 ± 0.08	0.06 ± 0.02
Lung	1.98 ± 0.24	0.95 ± 0.13	0.67 ± 0.07	0.08 ± 0.01
Kidney	25.09 ± 1.42	11.58 ± 2.46	5.78 ± 1.02	0.30 ± 0.04
Stomach	0.63 ± 0.15	0.56 ± 0.17	0.34 ± 0.20	0.08 ± 0.05
Intestine	22.45 ± 3.40	20.11 ± 7.22	8.66 ± 6.13	0.76 ± 0.42
Tumor	2.73 ± 0.67	2.03 ± 0.16	1.58 ± 0.42	0.59 ± 0.23
Muscle	1.04 ± 0.16	0.47 ± 0.13	0.30 ± 0.11	0.04 ± 0.02
Tumor/Blood	2.15 ± 0.39	3.51 ± 0.26	4.23 ± 0.81	13.13 ± 4.58

Organ uptake values are expressed as the percent injected dose per gram of tissue, except in the case of the stomach (the percent injected dose) and tumor/blood ratio. Values are represented as the mean ± S.D., n = 5.

Table 3. Blocking study of the biodistribution of ^{125}I-IBB in FM3A-implanted mice pretargeted with POS

Organ	Vehicle	IBB treatment
Blood	0.36 ± 0.18	0.48 ± 0.10
Liver	5.26 ± 0.61	2.58 ± 0.69*
Heart	0.76 ± 0.09	0.38 ± 0.08
Lung	1.09 ± 0.25	0.48 ± 0.12
Kidney	12.15 ± 5.03	2.44 ± 0.41**
Stomach	0.82 ± 0.48	0.25 ± 0.04
Intestine	9.04 ± 3.77	5.06 ± 2.30
Tumor	1.95 ± 0.63	0.90 ± 0.18*
Muscle	0.51 ± 0.06	0.16 ± 0.04†
Tumor/Blood	5.49 ± 1.12	1.93 ± 0.38‡

Organ uptake values are expressed as the percent injected dose per gram of tissue, except in the case of the stomach (the percent injected dose) and tumor/blood ratio. Values are represented as the mean ± S.D., $n = 5$.

*$P < 0.005$, **$P < 0.001$, †$P < 0.0005$, ‡$P < 0.0001$ vs. Vehicle group

Figures

Fig. 1

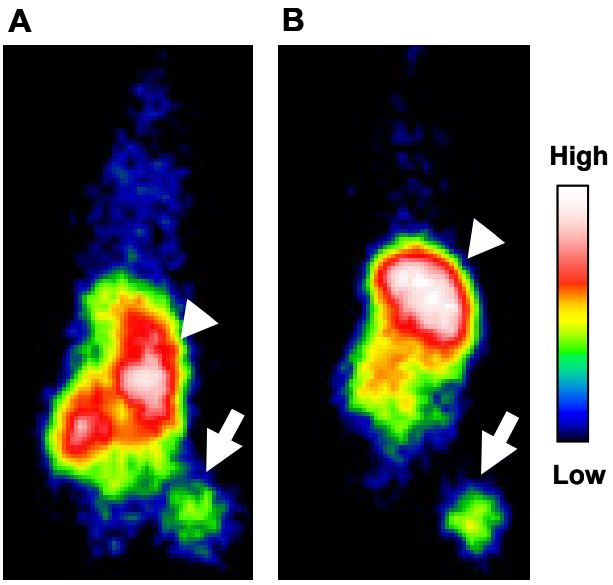

Typical planar images of FM3A-implanted mice, acquired through the pretargeting method (A) and the direct-targeting method (B). Images were acquired 6 h post-injection of ^{123}I-IBB in the pretargeting method and 24 h post-injection of ^{123}I-IPOS in the direct targeting method. Tumors were clearly visualized in a similar fashion in both images (arrow). Arrowheads indicate the intestine in A and the liver in B.

Fig. 2

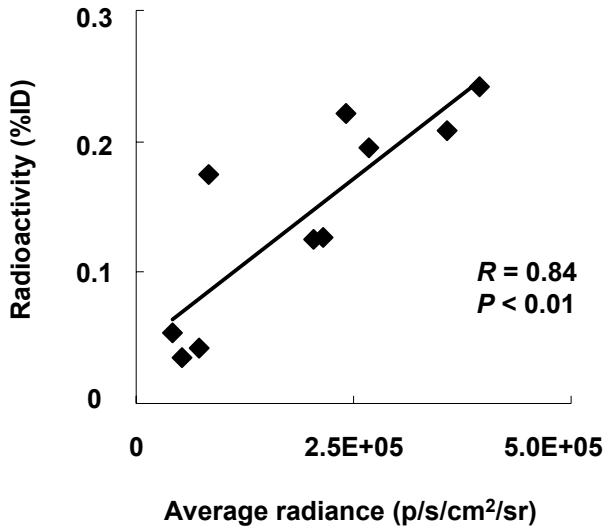

Correlation between ^{125}I-IBB accumulation and HIF-1 transcriptional activity within identical tumor in mice pretargeted with POS. Mice carrying tumors with the HIF-1-dependent luciferase reporter gene in both thighs were used. Ordinate represents accumulated radioactivity (%ID), and abscissa represents HIF-1-dependent luciferase bioluminescence. Correlation coefficient (R) was 0.84, indicating highly significant correlation ($P < 0.01$).

Fig. 3

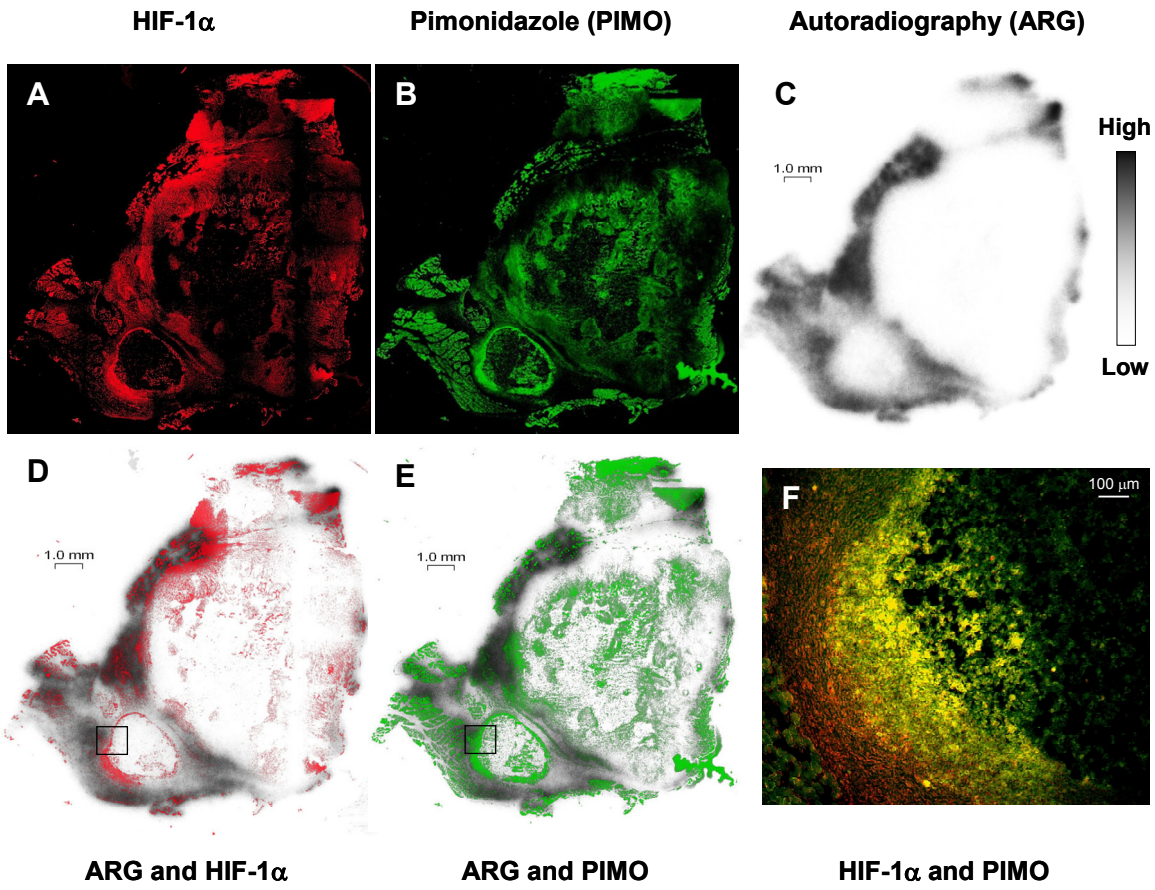

Comparison between the intratumoral distribution of ^{125}I-IBB and the HIF-1α- or the pimonidazole (PIMO)-positive hypoxic regions, in POS-pretargeted tumors. The typical images of HIF-1α immunostaining (A), PIMO immunostaining (B), and autoradiogram (ARG; C) in the identical section are shown. Merged images of ARG with HIF-1α immunostaining or PIMO immunostaining are also shown (D and E, respectively). A high-magnification merged image of HIF-1α immunostaining with PIMO immunostaining (F, from insets in D and E) show that some regions were both positive (*yellow*) while others did not match (*red* or *green*).

Fig. 4

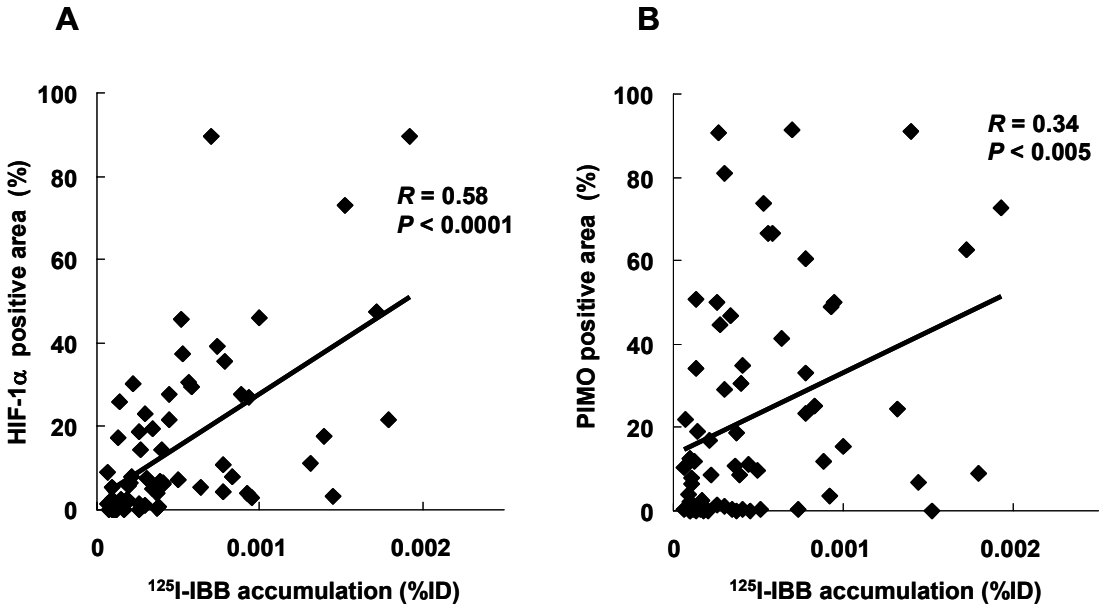

Correlation between ^{125}I-IBB accumulated area and HIF-1α- or PIMO-positive area in POS-pretargeted tumors. A total of 6 sections (1 section per tumor) were analyzed. Quantitative analysis of autoradiograms provided data *vis-à-vis* ^{125}I-IBB accumulation, expressed as %ID. A simple regression analysis of ^{125}I-IBB accumulation with HIF-1α or PIMO expression showed a directly proportional relationship (HIF-1α: $R = 0.58$, $P < 0.0001$; PIMO: $R = 0.34$, $P < 0.005$).